



CHORUS

This is the accepted manuscript made available via CHORUS. The article has been published as:

Multi-q Mesoscale Magnetism in CeAuSb₂

Guy G. Marcus, Dae-Jeong Kim, Jacob A. Tutmaher, Jose A. Rodriguez-Rivera, Jonas Okkels Birk, Christof Niedermeyer, Hannah Lee, Zachary Fisk, and Collin L. Broholm

Phys. Rev. Lett. **120**, 097201 — Published 28 February 2018

DOI: [10.1103/PhysRevLett.120.097201](https://doi.org/10.1103/PhysRevLett.120.097201)

Multi- q mesoscale magnetism in CeAuSb₂

Guy G. Marcus,^{1,*} Dae-Jeong Kim,² Jacob A. Tutmaher,¹ Jose A. Rodriguez-Rivera,^{3,4} Jonas Okkels Birk,^{5,6} Christof Niedermeyer,⁵ Hannah Lee,² Zachary Fisk,² and Collin L. Broholm^{1,4}

¹*Institute for Quantum Matter and Department of Physics and Astronomy,
The Johns Hopkins University, Baltimore, MD 21218, USA*

²*Department of Physics and Astronomy, University of California at Irvine, Irvine, California 92697, USA*

³*Department of Materials Sciences, University of Maryland, College Park, Maryland 20742, USA*

⁴*NIST Center for Neutron Research, Gaithersburg, MD 20899, USA*

⁵*Laboratory for Neutron Scattering and Imaging,*

Paul Scherrer Institut, CH 5232 Villigen-PSI, Switzerland

⁶*Department of Physics, Technical University of Denmark (DTU), DK-2800 Kgs. Lyngby, Denmark*

(Dated: January 26, 2018)

We report the discovery of a field driven transition from a single- q to multi- q Spin Density Wave (SDW) in the tetragonal heavy fermion compound CeAuSb₂. Polarized along \mathbf{c} , the sinusoidal SDW amplitude is $1.8(2) \mu_B/\text{Ce}$ for $T \ll T_N = 6.25(10)$ K with wavevector $\mathbf{q}_1 = (\eta, \eta, 1/2)$ ($\eta = 0.136(2)$). For $\mathbf{H} \parallel \mathbf{c}$, harmonics appearing at $2\mathbf{q}_1$ evidence a striped magnetic texture below $\mu_0 H_1 = 2.78(1)$ T. Above H_1 , these are replaced by coupled harmonics at $\mathbf{q}_1 + \mathbf{q}_2 = (2\eta, 0, 0) + \mathbf{c}^*$ until $\mu_0 H_2 = 5.42(5)$ T, where satellites vanish and magnetization non-linearly approaches saturation at $1.64(2) \mu_B/\text{Ce}$ for $\mu_0 H \approx 7$ T.

From micelles and vesicles in surfactant solutions [1, 2] to mixed phase type-II superconductors [3, 4], the spontaneous formation of large scale structure in condensed matter is a subject of great beauty, complexity, and practical importance. The phenomenon is often associated with competing interactions on distinct length scales and sensitivity to external fields that shift a delicate balance. Heavy fermion systems epitomize this scenario in metals, which place f -electrons with strong spin-orbit interactions near the transition between localized and itinerant [5, 6]. Whether their magnetism is described by oscillatory Ruderman-Kittel-Kasuya-Yosida (RKKY) exchange interactions between localized moments or by wavevector nesting involving f -electron Fermi-surfaces, these strongly interacting Fermi liquids are prone to the development of long wavelength modulation of spin and charge, and owing to the similarity of the f -electron bandwidth to the Zeeman energy scale there is strong sensitivity to applied magnetic fields.

Here we examine the magnetism of the heavy fermion system CeAuSb₂, which was previously shown to have two distinct ordered phases versus field (H) and temperature (T). By establishing the corresponding magnetic structures, we gain new insight into the mechanisms that give rise to the attendant electronic transport anomalies and control the overall phase diagram shown in Figure 1. Specifically, we show that the application of a magnetic field along the tetragonal axis of CeAuSb₂ induces a transition from a single- q to a multi- q magnetic texture, both \mathbf{c} -polarized and modulated on a length scale exceeding the lattice spacing by an order of magnitude.

CeAuSb₂ is a member of the ReTX₂ series of com-

pounds (Re=La, Ce, Pr, Nd, Sm; T=Cu, Ag, Au; X=Sb, Bi) [7–10]. They crystallize in spacegroup $P4/nmm$ (see inset to Figure 1) and commonly display metamagnetic transitions and magnetotransport anomalies, so our findings in CeAuSb₂ may have relevance throughout the series. CeAuSb₂ is Ising-like with an (001) easy axis and lattice parameters $a = 4.395$ Å and $c = 10.339$ Å at $T = 2$ K. The Néel temperature is $T_N = 6.25(10)$ K and the lower (upper) critical field between distinct magnetic phases is $\mu_0 H_1 = 2.78(1)$ T ($\mu_0 H_2 = 5.42(5)$ T) at low T (Figure 1) [11]. Superconductivity has not been reported for any compound in the ReTX₂ series and it is absent in CeAuSb₂ under applied pressure up to 5.5 GPa [12].

We grew high-purity single crystals of CeAuSb₂ via the self-flux method and used 8.5(1) mg and 114.5(1) mg crystals for diffraction in the (hhl) and ($hk0$) reciprocal lattice planes, respectively. To determine the magnetic structure, we mapped neutron diffraction intensity in the (hhl) and ($hk0$) planes using the MACS instrument at NIST [13]. The sample was rotated by 180 degrees about the vertical axis and the intensity data mapped to one quadrant. Field dependence with $\mathbf{H} \parallel \mathbf{c}$ was studied in the ($hk0$) plane on MACS with a vertical field magnet and in the (hhl) plane on RITA-II at PSI [14] using a horizontal field magnet. Absolute normalization was achieved by comparing nuclear diffraction to expectations for the accepted chemical structure [7], as described in the Supplementary Information.

The difference between diffraction data acquired below (2 K) and above (8 K) T_N is shown in Figure 2a. Three out of a quartet of satellite peaks are apparent around (111) and a single satellite is visible near the origin [15]. These peaks are indexed by $\mathbf{q}_1 = (\eta\eta 1/2)$ with $\eta = 0.136(2)$, indicating a long range ordered magnetic structure that doubles the unit cell along \mathbf{c} and

* email: guygma@jhu.edu

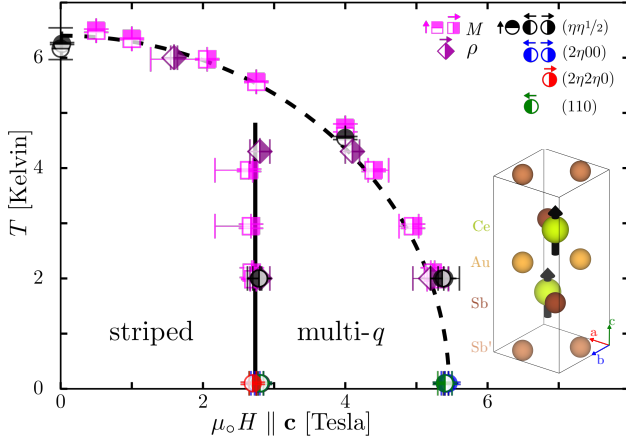


FIG. 1. Phase diagram for CeAuSb₂ with boundaries determined from magnetization (squares), resistivity (diamonds) and neutron diffraction (circles). (inset) Crystallographic unit cell of tetragonal CeAuSb₂. Magnetic moments shown on Ce sites illustrate the Γ_2 structure ($\uparrow\uparrow$) that is difficult to distinguish from the Γ_3 structure ($\uparrow\downarrow$) through neutron diffraction when the c -component of the magnetic wavevector is $1/2 c^*$.

is modulated in the basal plane with a wave length $\lambda_m = (a/\sqrt{2}\eta) = 23 \text{ \AA}$. The absence of satellite peaks of the form $(\eta, \eta, 1/2 + n)$, for integer $n \geq 1$ is consistent with diffraction from spins polarized along the c -axis as illustrated in Figure 1. To check this hypothesis and establish the size of the ordered moment, we extracted the intensity of magnetic Bragg peaks by integrating over the relevant areas of the two-dimensional intensity map in Figure 2a. The corresponding magnetic diffraction cross sections at $\mu_0 H = 0 \text{ T}$ are compared to a striped model with spins oriented along c in Figure 2c, which provides an excellent account of the data with a spin density wave amplitude of $m_{\mathbf{q}_1} = 1.8(2) \mu_B$. Note that these intensity data are insensitive to the relative phase between the fundamental and harmonic spin density waves and so cannot directly determine the real space spin structure.

Figure 3a reports the T -dependence of this ordered moment as extracted from the wave vector integrated magnetic neutron diffraction intensity at $(1 - \eta, 1 - \eta, 1/2)$ obtained by zero-field cooling (ZFC) to 100 mK. Near T_N these data can be described as $m_{\mathbf{q}_1}(T) \propto (1 - T/T_N)^\beta$ where $\beta = 0.32(5)$, consistent with the $\beta = 0.326$ for the 3D Ising model [16], but also with $\beta = 0.3645(25)$ for the 3D Heisenberg model [17]. Landau theory at such a second order phase transition predicts the magnetic structure forms a single irreducible representation (IR) of the little group, $\mathbf{G}_{\mathbf{q}}$, associated with a given wavevector. The \mathbf{q}_1 diffraction data are consistent with either Γ_2 ($\uparrow\uparrow$) or Γ_3 ($\uparrow\downarrow$). Here the arrows indicate the direction along c of the two spins within a unit cell (Figure 1).

Initial application of a magnetic field $\mathbf{H} \parallel c$ has little effect on the staggered magnetization, $m_{\mathbf{q}_1}$, until

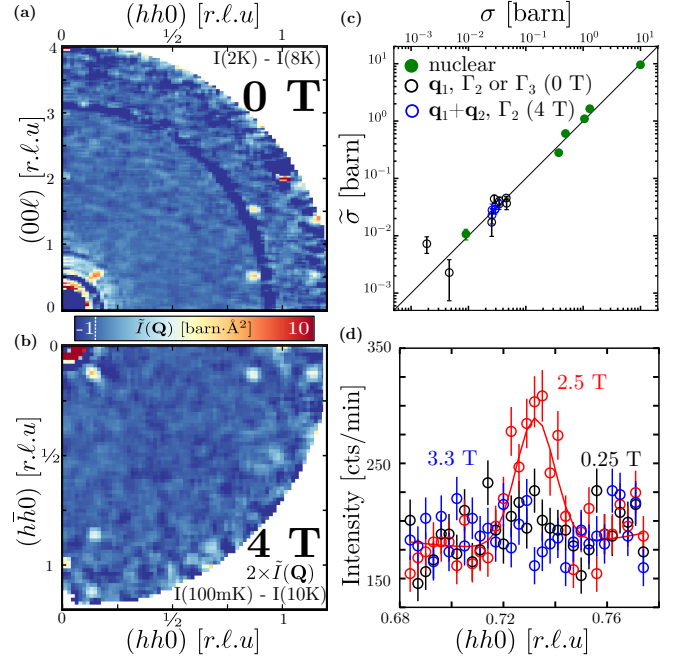


FIG. 2. Constant field maps of symmetrized, magnetic scattering cross-section for 0 T (a), and 4 T (b). The quality of nuclear and magnetic refinement of these data is demonstrated in (c). Experimental Bragg cross-sections ($\tilde{\sigma}$) are compared to the calculated cross-sections (σ) of a striped structure (\mathbf{q}_1) at 0 T and to a multi- q structure ($\mathbf{q}_1 \pm \mathbf{q}_2$) at 4 T. Panel (d) shows scans along $(hh0)$ in the (110) Brillouin zone at various fields illustrating the appearance of a harmonic peak for intermediate H .

an abrupt reduction by $0.65(5)\mu_B$ at $\mu_0 H_1 = 2.78(1) \text{ T}$ (Figure 3b). Continuing this isothermal field-sweep (IFS) to higher fields, $m_{\mathbf{q}_1}$ is continually suppressed before eventually falling below the detection limit above $\mu_0 H_2 = 5.42(5) \text{ T}$.

The characteristic wavevector exhibits clear hysteresis across H_2 . Figure 3(c,d) show that η locks into two distinct plateaus for increasing IFS each terminated by regimes where η , to within resolution, decreases continuously with increasing H . For decreasing IFS, η follows a different, non-intersecting trajectory without plateaus. This hysteresis in \mathbf{q}_1 persists to the lowest fields and for temperatures up to at least 2 K (see Supplementary Information), while no hysteresis is observed in the field dependence of the staggered magnetization (Figure 3b) or the uniform magnetization, m_0 (Figure 3e). For $T = 2 \text{ K}$, m_0 increases linearly with applied field at a rate of $m'_0 = 0.12(1)\mu_B T^{-1}/\text{Ce}$ until an abrupt increase of $\Delta m_0 = 0.23(3)\mu_B/\text{Ce}$ at H_1 . Above this transition, m_0 continues to increase linearly at a similar rate until H_2 , where the incommensurate magnetic peaks vanish. Interestingly, m_0 continues to increase for $H > H_2$ until saturating at $m_{0,\text{max}} = 1.64(2) \mu_B/\text{Ce}$. Extending to at least $H = 30 \text{ T}$ [11], this magnetization plateau indicates the magnetism of CeAuSb₂ is dominated by an

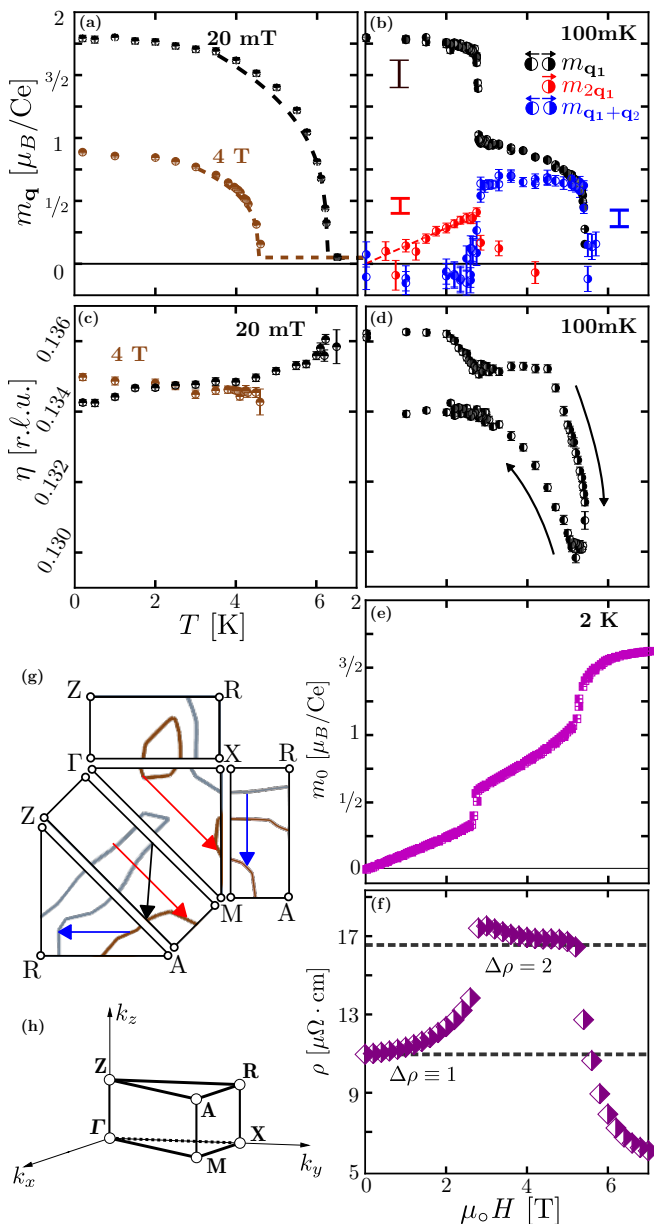


FIG. 3. The ordered magnetic Fourier amplitudes (a,b) and their corresponding wavevectors (c,d) throughout the H - T phase diagram. (e) Field dependence of the uniform magnetization. (f) Longitudinal magnetoresistance. The dashed lines highlight the factor two increase of $\Delta\rho$ across H_{c1} . The reduced Fermi surface (g) is extracted from DFT calculations and overlaid with potential nesting conditions for \mathbf{q}_1 (black), $2\mathbf{q}_1$ (red), and $\mathbf{q}_1 + \mathbf{q}_2$ (blue). A diagram of the reduced Brillouin zone is provided in (h).

isolated Kramer's doublet of the form $a|\pm 5/2\rangle \pm b|\mp 3/2\rangle$. Correspondingly, we expect the magnetization per Ce is capped near $m_{0,\max}$ even in the ordered state.

Figure 3f shows the longitudinal magnetoresistivity versus H at 2 K where $\rho(T)$ is dominated by the residual component. For $H = H_1$ there is an abrupt increase in resistivity that is subsequently reversed for $H > H_2$.

This decrease in ρ is approximately twice as large as the increase in ρ at H_1 . One interpretation is that parts of the Fermi surface develop a gap in the ordered regimes, and that this gapped area of the Fermi surface doubles for $H_1 < H < H_2$ compared to $H < H_1$ and vanishes for $H > H_2$.

Application of the $P4/nmm$ symmetry operations to \mathbf{q}_1 yields a second, symmetrically equivalent wavevector, $\mathbf{q}_2 = (\eta\bar{\eta}1/2)$. The observation of \mathbf{q}_1 satellite peaks for all $H < H_2$ leaves open whether distinct, single- q domains or a multi- q modulation describes magnetic structure in the various regimes. As we shall now show, this is resolved by analysis of field dependent magnetic diffraction data. Figure 2d shows representative line scans of elastic neutron diffraction along $(hh0)$ for $H < H_1$. We find a weak, field-induced peak at $(2\eta, 2\eta, 0) = 2\mathbf{q}_1 - \mathbf{c}^*$, which indicates the spatial modulation of magnetization ceases to follow a simple sinusoidal form in a field. The new Fourier component is supported by a single \mathbf{q}_1 domain and is not accompanied by harmonics of the form $\mathbf{q}_1 \pm \mathbf{q}_2$. This constitutes evidence that the $H < H_1$ SDW state is striped and consists of distinct \mathbf{q}_1 and \mathbf{q}_2 domains. Furthermore, the presence of a magnetic satellite peak at momentum transfer $\mathbf{Q} = (2\eta, 2\eta, 0)$ implies that for this Fourier component of the SDW the two Ce^{3+} sites within a unit cell contribute in phase. Thus, the second harmonic $m_{2\mathbf{q}_1}$ forms a representation of Γ_2 . This does not, however, constrain the fundamental modulation $m_{\mathbf{q}_1}$ for which both Γ_2 and Γ_3 are consistent with the data.

The field dependence of $m_{2\mathbf{q}_1}(H)$ is shown in Figure 3b. As directly apparent from Figure 2d, there is no evidence for this harmonic in zero field. A linear in H fit to $m_{2\mathbf{q}_1}(H)$ yields $m'_{2\mathbf{q}_1} = 0.14(2)\mu_B\text{T}^{-1}/\text{Ce}$, which is indistinguishable from m'_0 so that $|m_{2\mathbf{q}_1}(H)| \approx |m_0(H)|$ throughout the striped phase (Figure 3(b,e)). Combining the three Fourier components we obtain $m_j(\mathbf{r}) = m_0 + \nu^j m_{\mathbf{q}_1} \cos(\mathbf{q}_1 \cdot \mathbf{r}) + m_{2\mathbf{q}_1} \cos(2\mathbf{q}_1 \cdot \mathbf{r})$ on sublattice j , where $\nu = \pm 1$ encodes the lack of an experimental distinction between Γ_2 and Γ_3 for the \mathbf{q}_1 modulation. Without loss of generality, we pick $m_0 > 0$ and $m_{\mathbf{q}_1} > 0$. To ensure $|m_j(\mathbf{r})|$ does not exceed $m_{0,\max}$ defined by the Kramer's doublet ground state at any \mathbf{r} requires $m_{2\mathbf{q}_1} < 0$, so that $m_0(H) \approx -m_{2\mathbf{q}_1}(H)$. The corresponding $m_j(\mathbf{r}) = \nu^j m_{\mathbf{q}_1} \cos(\mathbf{q}_1 \cdot \mathbf{r}) + m_0(1 - \cos(2\mathbf{q}_1 \cdot \mathbf{r}))$ is shown in Figure 4a for H immediately below H_1 . Qualitatively, we find stripes where $m_j(\mathbf{r}) > 0$ broaden with field at the expense of stripes where $m_j(\mathbf{r}) < 0$. Given only the fundamental and second harmonics and assuming $m_{2\mathbf{q}_1} = -m_0$, a global maximum in $m_j(\mathbf{r})$ exceeding $m_{0,\max}$ would occur if m_0 were to exceed $m_{\mathbf{q}_1}/4$. The similarity of $m_0(H_1) = 0.32 \mu_B$ to $m_{\mathbf{q}_1}(H_1)/4 = 0.43(1) \mu_B$ indicates the phase transition at H_1 is associated with reaching the maximum magnetization possible for a striped phase with an individual Ce moment limited at $m_{0,\max}$ and the spatial modulation dominated by just three Fourier components m_0 , $m_{\mathbf{q}_1}$, and $m_{2\mathbf{q}_1}$.

Figure 3b shows $m_{2\mathbf{q}_1}$ abruptly vanishes for $H > H_1$. The false color map of the $(hk0)$ plane at $\mu_0 H = 4$ T in Figure 2b shows the $2\mathbf{q}_1$ harmonic is replaced by satellites spanned by $\mathbf{q}_1 \pm \mathbf{q}_2$ that surround (110) , $(\bar{1}\bar{1}0)$, and (000) . These indicate the simultaneous presence at the atomic scale of $m_{\mathbf{q}_1}$ and $m_{\mathbf{q}_2}$ and their interference term $m_{\mathbf{q}_1 \pm \mathbf{q}_2}$. Because the magnetic diffraction occurs for $\mathbf{Q} \perp \mathbf{c}^*$, we infer that $m_{\mathbf{q}_1 \pm \mathbf{q}_2}$ transforms as Γ_2 . Figure 3 shows $m_{\mathbf{q}_1 \pm \mathbf{q}_2}$ abruptly jumps to and then holds an essentially constant value of $0.7(1)\mu_B/\text{Ce}$ for $H_1 < H < H_2$. The similarity to the plateau-like dependence of the residual magneto-resistivity is consistent with both phenomena arising from the opening of an additional gap on the Fermi surface; two nesting wavevectors, rather than one, gap out twice as much of the Fermi surface, thereby doubling the residual resistivity as observed (Figure 3f).

For $H_1 < H < H_2$ the \mathbf{c} -oriented staggered magnetization can be described as

$$m_j(\mathbf{r}) = m_0 + \frac{1}{2}\nu^j m_{\mathbf{q}_1} [\cos(\mathbf{q}_1 \cdot \mathbf{r}) + \cos(\mathbf{q}_2 \cdot \mathbf{r})] \quad (1)$$

$$+ \frac{1}{2}m_{\mathbf{q}_1 \pm \mathbf{q}_2} [\cos((\mathbf{q}_1 + \mathbf{q}_2) \cdot \mathbf{r}) + \delta \cos((\mathbf{q}_1 - \mathbf{q}_2) \cdot \mathbf{r})].$$

Again, $\nu = \pm 1$ correspond to Γ_2 and Γ_3 , respectively, for the fundamental components. Although we expect only one to be realized, either is consistent with the present diffraction data *a priori*. m_0 and $m_{\mathbf{q}_1} = m_{\mathbf{q}_2}$ can again be chosen positive without loss of generality while $m_{\mathbf{q}_1 \pm \mathbf{q}_2} < 0$ is required to ensure $m_j(\mathbf{r}) < m_{0,\text{max}}$. The two qualitatively distinct magnetic textures for $\delta = \pm 1$ are illustrated in Figure 4(b,c). For $\delta = 1$, $m(\mathbf{r})$ describes a checkered pattern with four fold symmetry. The maximum Ce^{3+} moment in this structure is actually *reduced* relative to the striped phase immediately above H_1 (Figure 4d). In contrast, for the “woven” phase ($\delta = -1$) the measured Fourier amplitudes imply that $\max[m_j(\mathbf{r})]$ is field *independent* and pinned at $m_{0,\text{max}}$ throughout. While our diffraction does not provide definitive proof, this simple pattern that recalls the extended nature of the magnetization plateau makes the woven state an attractive hypothesis.

The woven SDW breaks the four-fold axis: lobes of \mathbf{c} -polarized spins extend along \mathbf{a} (b) for $m_{\mathbf{q}_1 \pm \mathbf{q}_2} > 0$ ($m_{\mathbf{q}_1 \pm \mathbf{q}_2} < 0$). Either between sub-lattices (Γ_3) or at the transition between unit cells along \mathbf{c} (Γ_2), the woven pattern shifts within the basal plane by half of its period in the direction of the prolate axis of the least magnetized lobes. As was the case for $H < H_1$, there remain two spatially separated domains only now composed of \mathbf{c} -polarized lobes of spins extending along either \mathbf{a} or \mathbf{b} .

The development of magnetization in the multi- q regime is qualitatively distinct from that in the low-field phase. This is apparent in Figure 3b where the fundamental amplitude $m_{\mathbf{q}_1}$ decreases with field at a rate of $m'_{\mathbf{q}_1} = -0.13(1)\mu_B \text{ T}^{-1}/\text{Ce}$ while the harmonic $m_{\mathbf{q}_1 \pm \mathbf{q}_2}$ is field independent and $m'_0 = 0.12(1)\mu_B \text{ T}^{-1}/\text{Ce}$ maintains the same value for $H > H_1$ as in the striped phase.

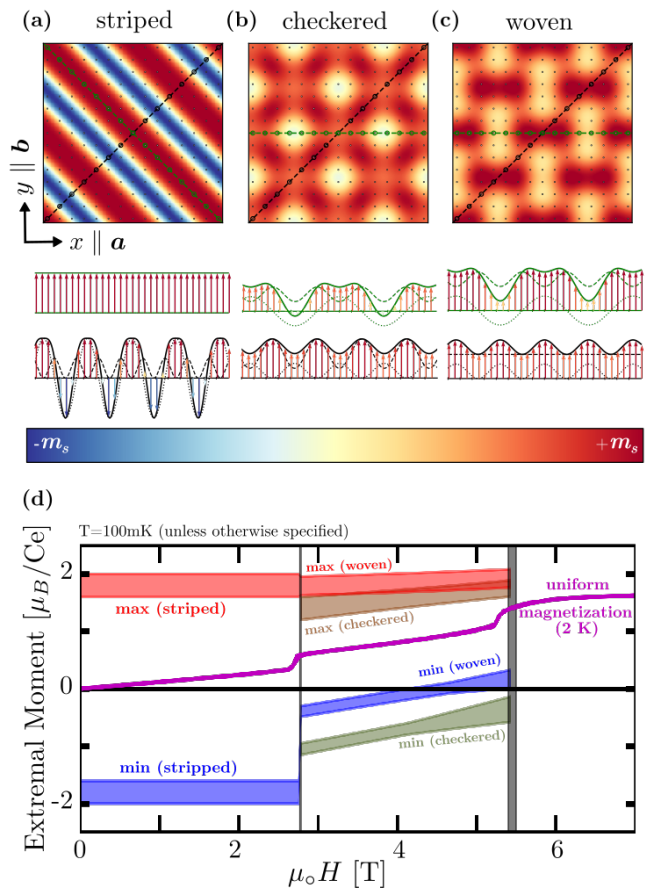


FIG. 4. (a) The low field striped magnetic structure. (b,c) Two possibilities for the high field multi- q structure. Throughout (a-c), the color scale indicates the component of magnetization along \mathbf{c} for a single square lattice layer of Ce atoms. False color images at the top of each panel show the magnetic structure within the basal plane while the lower frames show the modulation of magnetization along particular lines through the basal plane indicated above. (d) Maximum and minimum values of the local Ce^{3+} magnetization versus field as inferred from Figure 3 and these models.

Figure 4d shows that this corresponds to increasing the magnetization only of regions polarized antiparallel to \mathbf{H} .

Throughout the magnetization process, the magnetic wavelength, λ_m , varies by less than 5%, as seen in Figure 3(c,d). This contrasts with other cerium-based Ising systems. For example, CeSb undergoes a series of field driven phase transitions that alter the direction of magnetization of entire planes of spins from a $\uparrow\uparrow\downarrow\downarrow$ sequence ($q = (001/2)$), to $\uparrow\uparrow\downarrow\downarrow\uparrow\uparrow\downarrow$ ($q = (004/7)$), to $\uparrow\uparrow\downarrow\uparrow\uparrow\downarrow$ ($q = (002/3)$), all the way to full ferromagnetism ($q = 0$) [18]. These square-wave structures are characterized by a strong third order harmonic and their magnetic $4f$ -electrons can be modeled as localized Ising degrees of freedom subject to oscillatory RKKY interactions.

A model of competing near neighbor exchange interactions that reproduces the critical wave vectors \mathbf{q}_1 and \mathbf{q}_2 , the Weiss temperature, and the upper critical field

is possible for CeAuSb₂. At a minimum, it involves antiferromagnetic $J_c > 0$ between Ce sites on the **c**-bond and basal-plane interactions $J_1 > 0$ on the **a**-bond, $J_2 < J_1/4$ on the (**a** + **b**)-bond, and $J_3 = -J_1/4 \cos 2\pi\eta$ on the 2**a**-bond [19]. In such a local-moment model for CeAuSb₂, a third order harmonic of $0.60(7)_B$ would be expected. However, our data establish a quantitative limit of $|m_{3\mathbf{q}_1}| < 0.1\mu_B$. This precludes square-wave modulation for $H < H_1$ and points to an itinerant description that nonetheless upholds the limits on Ce polarization set by its crystal field ground state. To examine the possibility of Fermi surface (FS) nesting induced SDW, we calculated the FS using the generalized gradient approximation (Figure 3g). Near the Fermi level, the band structure is dominated by *f*-electrons with an order of magnitude smaller contribution to the density of states coming from strongly dispersive *p*-bands. While there are no ideal nesting conditions, \mathbf{q}_1 , $2\mathbf{q}_1$, and $\mathbf{q}_1 \pm \mathbf{q}_2$ do connect areas of the quasi-2D FS that extend along **c**, consistent with an SDW instability.

The distinct hysteresis of the SDW wave vector shown in Figure 3d versus field indicates a truly incommensurate modulation and a profound rearrangement of static magnetism at H_1 and H_2 . Upon reducing field at low *T*, nucleation of the multi-*q* state from the paramagnetic state at H_2 can be expected to allow for greater adherence to constraints imposed by impurities and defects than when nucleating the multi-*q* state from within the striped state upon increasing field past H_1 . Within the SDW picture, the corresponding subtle differences in magnetic order provide a natural explanation for weakly field-hysteretic electronic transport [11, 20] [21].

Our results provide a phenomenological description of the magnetization process in CeAuSb₂ that links the critical magnetization at the metamagnetic transitions to the limited dipole moment of a Ce³⁺ Kramer's doublet. Net magnetization is achieved by adding both a uniform and a single harmonic component to a sinusoidal magnetization wave while maintaining the fundamental wave length and maximum amplitude. Despite these local moment features, the absence of a third harmonic at low *T* suggests Kondo-like screening or a fully itinerant picture will be appropriate as we seek a unified understanding of the meta-magnetic transitions in the ReTX₂ family of heavy fermion compounds.

We are glad to thank Christian Batista, Martin Mourigal, Sid Parameswaran, Chandra Varma, Yuan Wan, and Andrew Wills for helpful discussions. This research was funded by the U.S. Department of Energy, Office of Basic Science, Division of Materials Sciences and Engineering, Grant No. DE-FG02-08ER46544. GGM acknowledges generous support from the NSF-GRFP, Grant No. DGE-1232825.

-
- [1] E. W. Kaler, A. K. Murthy, B. E. Rodriguez, and J. A. Zasadzinski, *Science* **245**, 1371 (1989).
 - [2] S. A. Safran, P. Pincus, and D. Andelman, *Science* **248**, 354 (1990).
 - [3] G. Blatter, M. V. Feigel'man, V. B. Geshkenbein, A. I. Larkin, and V. M. Vinokur, *Reviews of Modern Physics* **66**, 1125 (1994).
 - [4] B. Rosenstein and D. Li, *Reviews of Modern Physics* **82**, 109 (2010).
 - [5] S. Hoshino and Y. Kuramoto, *Physical Review Letters* **111**, 026401 (2013).
 - [6] Z. Fisk, H. Ott, T. Rice, and J. Smith, *Nature* **320**, 124 (1986).
 - [7] O. Sologub, K. Hiebl, P. Rogl, H. Noël, and O. Bodak, *Journal of Alloys and Compounds* **210**, 153 (1994).
 - [8] C. Adriano, P. F. S. Rosa, C. B. R. Jesus, J. R. L. Mardegan, T. M. Garitezi, T. Grant, Z. Fisk, D. J. Garcia, A. P. Reyes, P. L. Kuhns, R. R. Urbano, C. Giles, and P. G. Pagliuso, *Physical Review B* **90**, 235120 (2014).
 - [9] S. M. Thomas, P. F. S. Rosa, S. B. Lee, S. A. Parameswaran, Z. Fisk, and J. Xia, *Phys. Rev. B* **93**, 075149 (2016).
 - [10] E. M. Seibel, W. Xie, Q. D. Gibson, and R. J. Cava, *Journal of Solid State Chemistry* **230**, 318 (2015).
 - [11] L. Balicas, S. Nakatsuji, H. Lee, P. Schlottmann, T. P. Murphy, and Z. Fisk, *Physical Review B* **72**, 064422 (2005).
 - [12] S. Seo, V. A. Sidorov, H. Lee, D. Jang, Z. Fisk, J. D. Thompson, and T. Park, *Physical Review B* **85**, 205145 (2012).
 - [13] J. A. Rodriguez, D. M. Adler, P. C. Brand, C. Broholm, J. C. Cook, C. Brocker, R. Hammond, Z. Huang, P. Hundertmark, J. W. Lynn, N. C. Maliszewskyj, J. Moyer, J. Orndorff, D. Pierce, T. D. Pike, G. Scharfstein, S. A. Smee, and R. Vilaseca, *Measurement Science and Technology* **19**, 034023 (2008).
 - [14] K. Lefmann, C. Niedermayer, A. B. Abrahamsen, C. R. H. Bahl, N. B. Christensen, H. S. Jacobsen, T. L. Larsen, P. Häflicher, U. Filges, and H. M. Rønnow, *Physica B: Condensed Matter* **385-386**, 1083 (2006).
 - [15] The $(1+\eta, 1+\eta, 1.5)$ location lies at the limit of detector coverage where statistical error is enhanced.
 - [16] A. Pelissetto and E. Vicari, *Physics Reports* **368**, 549 (2002).
 - [17] J. C. Le Guillou and J. Zinn-Justin, *Phys. Rev. B* **21**, 3976 (1980).
 - [18] T. Chattopadhyay, P. Bulet, J. Rossat-Mignod, H. Bartholin, C. Vettier, and O. Vogt, *Phys. Rev. B* **49**, 15096 (1994).
 - [19] L. Seabra, P. Sindzingre, T. Momoi, and N. Shannon, *Physical Review B* **93**, 085132 (2016).
 - [20] L. Zhao, E. A. Yelland, J. A. N. Bruin, I. Sheikin, P. C. Canfield, V. Fritsch, H. Sakai, A. P. Mackenzie, and C. W. Hicks, *Phys. Rev. B* **93**, 195124 (2016).
 - [21] See Supplemental Material [url] for supporting measurements and general experimental details, which includes Refs. [22–29].
 - [22] J. Rodríguez-Carvajal and F. Bourée, *EPJ Web of Conferences* **22**, 00010 (2012).
 - [23] A. S. Wills, *Physica B: Condensed Matter* **276-278**, 680 (2000).

- [24] G. Kresse and J. Furthmuller, *J. Comp. Materials* **6**, 15 (1996).
- [25] G. Kresse and J. Furthmuller, *Phys. Rev. B* **54**, 11169 (1996).
- [26] G. Kresse and J. Hafner, *Phys. Rev. B* **47**, 558 (1993).
- [27] J. P. Perdew, A. Ruzsinszky, G. I. Csonka, O. A. Vydrov, G. E. Scuseria, L. A. Constantin, X. Zhou, and K. Burke, *Phys. Rev. Lett.* **100**, 136406 (2008).
- [28] J. K. Jang and J. Y. Rhee, *Current Applied Physics* **16**, 475 (2016).
- [29] T. Jeong, *Physica B* **388**, 249 (2007).